Yield of $2p\sigma$ molecular-orbital x rays in heavy-ion collisions*

R. Anholt and W. E. Meyerhof
Department of Physics, Stanford University, Stanford, California 94305
(Received 12 May 1977)

This paper examines the spectral yield of molecular-orbital (MO) x rays observed in asymmetric 470-MeV Xe collisions. According to a proposal by Heinig *et al.*, x-ray transitions to $2p\sigma$ vacancies occurring during the collision give an intense continuum spectrum which falls off rapidly above the K x ray lines emitted by the heavier collision partner. Dynamical calculations of the $2p\sigma$ MO x-ray thick-target yield indeed agree within a factor of 3 with the observed intensity. The velocity and impact-parameter dependence of $2p\sigma$ MO x-ray production are discussed.

I. INTRODUCTION

Studies of noncharacteristic continuum x rays in heavy-ion–atom encounters at energies between 0.5 and 3 MeV per nucleon have revealed two distinct continua above the K x-ray lines emitted by the heavier collision partner.[1] The higher x-ray energy continuum, $C2$ in Fig. 1, is thought to be due mostly to K molecular-orbital (MO) x rays (transitions to vacancies in the $1s\sigma$ MO). Recently, Heinig *et al.*[2] suggested that the lower energy and more intense continuum, $C1$ in Fig. 1, is due to transitions to vacancies in the $2p\sigma$ MO. They call this $2p\sigma$ MO x-ray radiation intermediate L-K MO x rays.

In a second paper, Heinig *et al.*[3] performed dynamical calculations of the $2p\sigma$ MO x-ray intensity in symmetric Ni+Ni, Ge+Ge, and Nb+Nb collisions. They found agreement with the shape and, within a factor of 3, with the experimental intensity of $C1$ continuum x rays. Hence there can be little doubt that their hypothesis about the origin of the $C1$ continuum is correct. Additional confirmation has come from the measurement of the Doppler shift of these x rays which indicates that the radiation is emitted by the quasimolecule.[4]

Several questions about $2p\sigma$ MO x-ray emission were only partially answered in Ref. 3. Heinig *et al.* neglected the time dependence of the amplitude for creating a $2p\sigma$ vacancy. The emission of $2p\sigma$ MO x rays supposedly occurs in a one-collision process in which a vacancy is made in the $2p\sigma$ MO and radiates later in the same collision. Heinig *et al.* assume that the vacancy is made instantly at the turning point of the first collision ($t=0$), neglecting the fact that the amplitude $a(t)$ for making a $2p\sigma$ vacancy has a complicated dependence on time. Thorson and Choi[5] have shown that the time dependence of $a(t)$ affects the one-collision $1s\sigma$ MO x-ray yield in a marked way. Therefore, one may wonder how important it is in the one-collision emission of $2p\sigma$ MO x rays.

We also wished to investigate the dependences of the intensity of $2p\sigma$ MO x rays on the ion velocity and the collision impact parameter. These quantities were not reported in Ref. 3.

The extremum in the $2p\sigma$ binding energy at intermediate internuclear distances (see Fig. 1) suggests that one should observe satellite peaks in the continuum spectrum. In the quasistatic or stationary phase model of MO x-ray emission,[6] the cross section is inversely proportional to dE/dR, the derivative of the transition energy with respect to internuclear distance R. Thus if the derivative

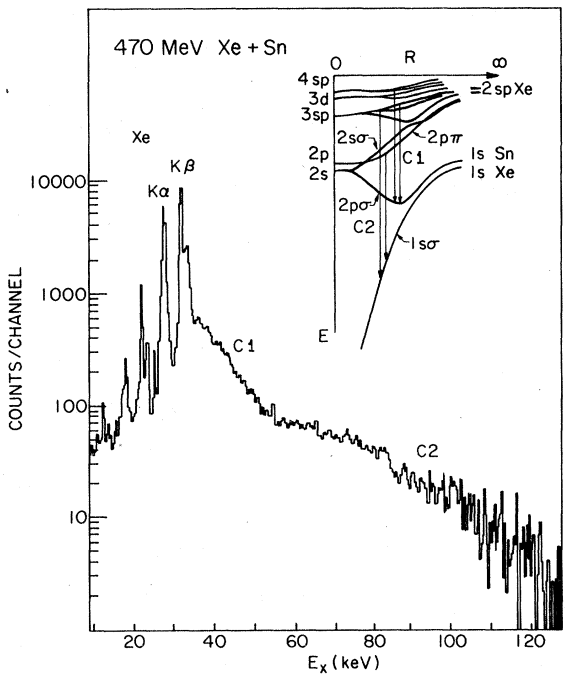

FIG. 1. Continuum spectrum observed in 470–MeV Xe+Sn encounters. Inset shows qualitative MO correlation diagram. Continua $C1$ and $C2$ are thought to be due to x-ray transitions to vacancies in the $2p\sigma$ MO and in the $1s\sigma$ MO, respectively.

goes to zero at some internuclear distance R_0, a peak (or peaks) in the x-ray spectrum should be observed at the transition energy $E_x = E_{2p\sigma}(R_0) - E_f(R_0)$, where E_f is the binding energy of the final state. These peaks are known in studies of line broadening in hot plasmas.[7] Dynamical effects in such systems reduce the sharp peaks to broad bands. Therefore, we wondered whether there is any evidence for these peaks in studies of $2p\sigma$ MO x-ray continua, and what the effects of dynamical broadening might be.

A final motivation for the present work is the study of $2p\sigma$ MO x rays in asymmetric collisions. Data were taken for 470-MeV Xe over a wide range of target atomic numbers.[8] A clear separation of the two continua was obtained.

Section II of this paper outlines the method employed to perform dynamical calculations of the $2p\sigma$ MO x-ray yield. Our calculations differ from those made by Heinig *et al.*[3] Details concerning the amplitude for creating $2p\sigma$ vacancies, the x-ray transition energies, and the dipole matrix elements can be found in Sec. II also. The results, together with discussions of the questions posed in the above paragraphs, are included in Sec. III.

II. CALCULATIONS OF THE SPECTRAL YIELD

A. General theory

The method used for calculating the $2p\sigma$ MO x-ray cross section is essentially the same method used by Weisskopf,[9] Macek and Briggs,[10] and Anholt.[11] The dipole velocity matrix element $D_f(R(t))$ between the $2p\sigma$ state and state f is Fourier analyzed:

$$D_{fi}(\omega_x) = \frac{1}{(2\pi)^{1/2}} \int_{-\infty}^{\infty} dt A_i(t) D_f(R(t)) \exp\left\{ i \int_0^t [\omega_x - \omega_{2p\sigma}(t') + \omega_f(t')]\, dt' \right\}, \tag{1}$$

where $A(t)$ is the amplitude for having a $2p\sigma$ vacancy, $\hbar\omega_x$ is the x-ray energy, and $\hbar\omega_{2p\sigma}$ and $\hbar\omega_f$ are the energies of the $2p\sigma$ state and state f, which depend on internuclear distance. The Fourier transform $D_{fi}(\omega_x)$ depends on the ion velocity v, impact parameter b, and, through $A_i(t)$, on the state i to which the $2p\sigma$ electron is excited. The cross section for an x-ray transition from state f is given by integrating over impact parameters and summing over higher states i:

$$\frac{d\sigma_f}{dE_x}(E_x, v) = \frac{4e^2\omega_x}{3\hbar c^3} \sum_i \int_0^{\infty} 2\pi b\, db\, |D_{fi}(\omega_x)|^2 . \tag{2}$$

Following Macek and Briggs[10] and Anholt,[11] $\omega_{2p\sigma}(t') - \omega_f(t')$ is separated into $\omega_0 + \Delta\omega(t')$ where $\omega_0 = \omega_{2p\sigma}(\infty) - \omega_f(\infty)$. The integral over time is separated into two contributions: one from the contribution to $D_{fi}(\omega_x)$ occurring for times before and during the first collision ($t \leq T$) and the remaining contribution occurring from times after the first collision ($t > T$). The amplitude $A_i(t)$ is separated into a product $a_i \exp(-\lambda t/2)$ where λ is the phenomenological radiative and Auger decay rate for the $2p\sigma$ vacancy (taken as a constant[11]) and $a_i(t)$ is the amplitude for having collisionally excited a $2p\sigma$ electron to state i. The quantity $D_{fi}(\omega_x)$ is then partially integrated to obtain

$$(2\pi)^{1/2} D_{fi}(\omega_x) = [i(\omega_x - \omega_0) + \tfrac{1}{2}\lambda]^{-1} \left\{ \int_{-\infty}^{T} dt [\dot{a}D + \dot{D}a - i\Delta\omega a D] \exp\left(i \int_0^t [\omega_x - \omega_0 - \Delta\omega(t') + \tfrac{1}{2} i\lambda]\, dt' \right) \right.$$
$$\left. + a(\infty) \int_T^{\infty} dt\, (\dot{D} - i\Delta\omega D) \exp\left(i \int_0^t [\omega_x - \omega_0 - \Delta\omega(t') + \tfrac{1}{2} i\lambda]\, dt' \right) \right\} , \tag{3}$$

where the quantities $a \equiv a_i(t)$, $\dot{a} \equiv da_i/dt$, $D \equiv D_f(R(t))$, and $\dot{D} \equiv dD_f/dt$ all depend on time or internuclear distance.

Heinig *et al.*[3] discuss the presence of a pure separated-atom (SA) Lorentzian in their equations of the form

$$D_c(\omega_x) = D(0)/[i(\omega_x - \omega_0) + \tfrac{1}{2}\lambda] . \tag{4}$$

This Lorentzian gives a spectral intensity considerably larger than experiment for x-ray energies above the united-atom (UA) K transition energy.[3] The advantage of Eq. (3) is that no SA Lorentzian is present.

The first term in Eq. (3) gives the one-collision MO x-ray intensity; the second gives the two-collision MO x-ray intensity.[6,11] These contributions can be added incoherently since the phase relationship between radiation emitted in the first and subsequent collisions is lost in integrating over impact parameters and averaging over free path

lengths (except in experiments with oriented single crystals[12]). We need not consider the two-collision contribution to $2p\sigma$ MO x-ray production. The two-collision $1s\sigma$ or $2p\sigma$ MO x-ray yield differs from the one-collision contribution by a factor of the order of $\pi n_2 R^2 v\tau$, where n_2 is the target atom density, τ is the projectile K-vacancy lifetime, and R is the maximum internuclear distance at which the vacancy can radiate a photon with energy E_x in the quasistatic model.[6] For 470-MeV Xe + Sn encounters, $\pi R^2 n_2 v\tau$ is of the order of 10^{-5} which is clearly negligible. In the production of $1s\sigma$ MO x rays, the two-collision process is important because the cross section for the creation of $1s\sigma$ vacancies is smaller by a factor of 10^{-3} to 10^{-6} than the cross section for the creation of $2p\sigma$ vacancies. Therefore there is a clear advantage in making projectile K vacancies in the $2p\sigma$ MO, then transferring them to the $1s\sigma$ MO in a second collision.

Details concerning the calculation of $a_i(t)$, $D(R(t))$, and $\omega_0 + \Delta\omega(t)$ are discussed in the following subsections. Using these quantities, Eq. (3) was numerically integrated and the cross section was found using Eq. (2). We measured thick-target yields of continuum x rays. To compare with experiment, the radiation cross section was divided by the cross section for the production of $2p\sigma$ vacancies and was multiplied by the experimental thick-target yield of $2p\sigma$ vacancies $Y_{2p\sigma}$:

$$\frac{dY}{dE_x} \simeq Y_{2p\sigma} \frac{d\sigma}{dE_x} \frac{1}{\sigma_{2p\sigma}} . \tag{5}$$

In the notation of Eq. (3), the $2p\sigma$ cross section is given by

$$\sigma_{2p\sigma} = \sum_i \int 2\pi b\, db\, |a_i(\infty)|^2 . \tag{6}$$

This approximation is discussed further below.

B. $2p\sigma$ vacancy production

Projectile and target thick-target K-vacancy yields plotted against target atomic number Z_2 are shown in Fig. 2.[13] The $2p\sigma$-vacancy yield is given approximately by summing the yield of projectile and target K vacancies.[13] The cross section for the production of $1s\sigma$ vacancies is equal to the projectile K-vacancy cross section for $Z_2 \lesssim 30$, and is equal to the target cross section for $Z_2 \gtrsim 80$. The yield of $1s\sigma$ vacancies is at least a factor of 10^{-2} smaller than the $2p\sigma$ yield. For $30 \lesssim Z_2 \lesssim 80$, the yield of higher-$Z$ K vacancies is mainly due to the sharing of outgoing $2p\sigma$ vacancies between the higher- and lower-Z collision partners.[13,14] Hence as Z_L approaches Z_H, the yield of vacancies in the higher-Z partner rises above the $1s\sigma$-vacancy yield.

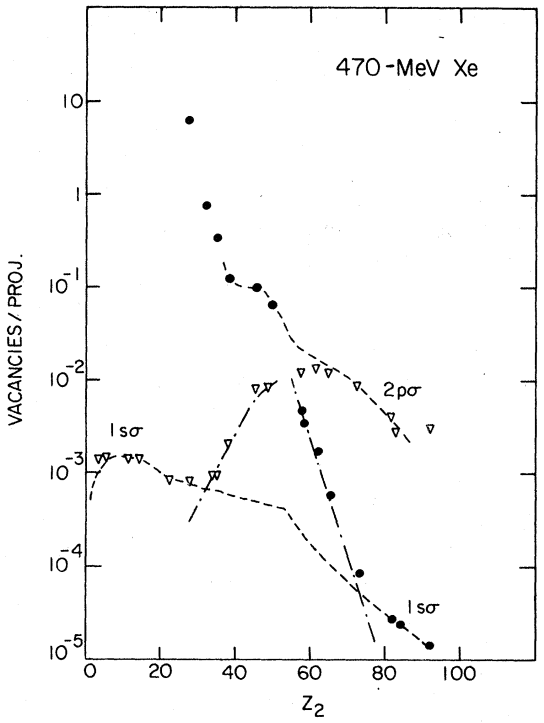

FIG. 2. Projectile (▽) and target (●) thick-target K-vacancy yields. Dashed lines show schematically the yield of vacancies created in the $2p\sigma$ and $1s\sigma$ MO's. Dash-dot line shows the yield of $2p\sigma$ vacancies shared with the higher-Z collision partner on the outgoing part of the collision.

Meyerhof *et al.*[14] showed that $2p\sigma$-vacancy formation in solid targets predominantly occurs via a multiple-collision process. Projectile $2p$ vacancies made in one collision live long enough to enter the $2p\pi$ MO in a second collision where rotational coupling transfers the vacancy to the $2p\sigma$ MO.[15] The cross section for the production of $2p\sigma$ vacancies is given by

$$\sigma_{2p\sigma} \approx \tfrac{1}{3}\sigma_{2px}^{\text{proj}}\, n_2 v \tau_{2px} w_{2p} \sigma_{\text{rot}} , \tag{7}$$

where $\sigma_{2px}^{\text{proj}}$ is the cross section for the production of projectile L_2 and L_3 x rays, τ_{2px} is the radiative decay rate for projectile $2p$ vacancies, w_{2p} describes the probability that a projectile $2p$ vacancy will couple to the $2p\pi$ MO, and σ_{rot} is the rotational coupling cross section. The quantity $\sigma_{2px} n_2 v \tau_{2px} w_{2p}$ is independent of time and impact parameter. The factor w_{2p} may depend on impact parameter, but like K-vacancy sharing,[16] it is probably constant over the range of impact parameters where the maximum contribution to σ_{rot} occurs.

Therefore to obtain $a_i(t)$ in Eq. (3), we need only solve coupled differential equations for the transfer of a single $2p\sigma$ electron into the $2p\pi_x$ MO (or a

$2p\pi$ vacancy to the $2p\sigma$ MO). [The quantity $\sigma_{2px} n_2 v \tau_{2px} w_{2p}$ is accounted for in using Eq. (5).] These equations are well known[17-19]:

$$\dot{c}_2(t) = -c_1(t)(bv/R^2)f(R) \times \exp\left(i\int^t [\omega_{2p\pi}(t') - \omega_{2p\sigma}(t')]dt'\right),$$
$$\dot{c}_1(t) = c_2(t)(bv/R^2)f(R) \times \exp\left(-i\int^t [\omega_{2p\pi}(t') - \omega_{2p\sigma}(t')]dt'\right), \quad (8)$$

where c_2 refers to the $2p\pi_x$ state and c_1 refers to the $2p\sigma$ state, R is the internuclear distance, and $f(R) = \langle 2p\sigma | \partial/\partial\theta | 2p\pi_x \rangle$. The initial conditions are

$$c_1(-\infty) = 1, \quad c_2(-\infty) = 0.$$

With these conditions the rotational cross section is given by

$$\sigma_{\rm rot} = \int 2\pi b\, db\, P(b), \quad (9)$$

where $P(b) = |c_2(+\infty)|^2$. In Eq. (3), $a_i(t)$ is equal to $c_2(t)$.

To solve these equations three approximations are made: (i) The Gershtein-Krivchenkov formula[20] for the $2p\pi$-$2p\sigma$ binding energy difference is used:

$$\omega_{2p\pi}(R) - \omega_{2p\sigma}(R) = kR^2, \quad (10)$$

where

$$k = \tfrac{1}{40} Z_1 Z_2 (Z_1 + Z_2)^2 (e^2/a_0^3\hbar).$$

(ii) The $2p\sigma$-$2p\pi$ radial overlap $f(R)$ is set equal to unity.[18,19] (iii) Equations (8) and (3) are integrated along straight-line trajectories.

The use of these approximations to calculate $\sigma_{\rm rot}$ has been examined previously.[19] In essence, calculations of $P(b)$ above the threshold[17] agree within 30% with Taulbjerg's more accurate calculations[18] except in the region of the kinematic peak where the use of straight-line trajectories breaks down. However, this peak does not contribute much to the cross section. Since our radiation cross section is divided by $\sigma_{\rm rot}$ (calculated using the same approximations), the errors generated in making these approximations tend to cancel.

C. Dipole matrix elements and energy levels

We calculated $2p\sigma$ dipole transition matrix elements and energy levels using nonrelativistic one-electron two-center wave functions.[21] To display the dependence of $D(R)$ on R, it is more meaningful to show transition rates $\lambda(R)$ where

$$\lambda(R) = (4e^2/3\hbar c^3)(\omega_{2p\sigma} - \omega_f)|D_f(R)|^2. \quad (11)$$

Transition rates to several MO's in Xe + Sn encounters are shown in Fig. 3. Corresponding energy levels are shown in Fig. 4.

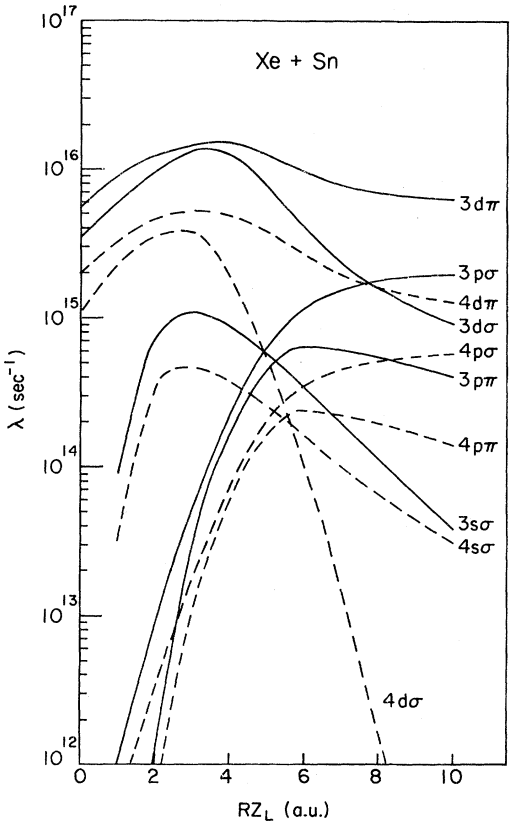

FIG. 3. Xe + Sn radiative transition rates between the $2p\sigma$ MO and various other MO's vs reduced internuclear distance (Z_L is the lower Z). The rates were calculated using one-electron wave functions and binding energies.

In the heavy-ion–atom encounters examined below, the $2p\sigma$ continuum radiation is observed above the UA L x-ray lines. Hence small internuclear distances ($RZ_L \lesssim 5$ a.u.) are expected to be important.[6] At these distances transitions rates to the $d\sigma$ and $d\pi$ MO's are largest; the transition rates to the $s\sigma$, $p\sigma$, and $p\pi$ MO's are significant only at large internuclear distances. Fourier analyzing all of these transition matrix elements would consume an inordinate amount of computer time. Hence four additional approximations are made:

(i) Transitions to the $s\sigma$, $p\sigma$, and $p\pi$ MO's are neglected. Only transitions to the $3d\sigma$, $3d\pi$, $4d\sigma$, and $4d\pi$ MO's are considered.

(ii) The binding energy of the final state, $\hbar\omega_f$ in Eq. (1), is set equal to the experimental UA binding energy for that level. Figure 4 shows that the $d\pi$ energy level is nearly constant and equal to the UA (one-electron) value. The approximation is less accurate for the $d\sigma$ levels. For instance the

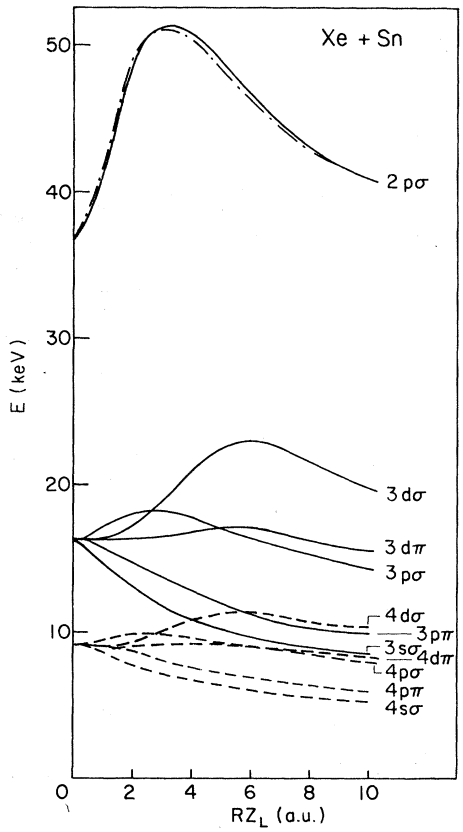

FIG. 4. One-electron molecular binding energies for Xe + Sn vs internuclear distance. Dash-dot line was calculated using Eq. (12) as described in text.

$3d\sigma$ energy level varies by as much as 5 keV (35%) from the one-electron UA value. However, in the many-electron molecule, the UA $3d\sigma$ binding energy is equal to 5 instead of 16 keV. Assuming the shape of the $3d\sigma$ curve to be approximately unaltered, a 35% change in $E_{3d\sigma}$ will only be 1.5 keV in the many-electron molecule, and its neglect represents a 4% error in $E_{2p\sigma} - E_{3d\sigma}$.

(iii) One-electron calculations of $E_{2p\sigma}(R)$ do not reproduce the actual $2p\sigma$ binding energy sufficiently accurately for this work. To compensate partially for this, we expressed $E_{2p\sigma}(R)$ as

$$E_{2p\sigma}(R) = E_s + (E_u - E_s)\exp(-0.12R) + 3R_p\{1 - \exp[-0.3835(QR)^2]\} \times \exp(-0.115QR), \quad (12)$$

with $R_p = (-0.165 + 0.367\sqrt{Q})E_s$ and $Q = Z_H/Z_L$ is the ratio of atomic charges. For the energies E_u and E_s we used experimental UA $2p_{1/2}$ and lower-Z SA $1s_{1/2}$ binding energies, respectively. This assures us that the $2p\sigma$ binding energy approaches the correct limits at $R=0$ and $R=\infty$. We cannot be certain that $E_{2p\sigma}(R)$ is accurate between these two limits, but observe that if one-electron values of E_u and E_s are used, Eq. (12) accurately reproduces molecular one-electron calculations (see dashed line in Fig. 4).

(iv) Since the one-electron values of $\lambda(R)$ differ from the many-electron values, we multiply $d\sigma/dE_x$ by $\lambda^M_{UA}/\lambda^0_{UA}$ where λ^M_{UA} is the many-electron value of the total UA $2p_{1/2}$ radiative transition rate[22] and λ^0_{UA} is the one-electron value. This correction is of the order of 0.8.

III. RESULTS

Figure 5 compares thick-target yields of $2p\sigma$ MO x rays with spectra observed in 470-MeV Xe bombardments of Cd, Sn, and Pr. The estimated one-collision $1s\sigma$ MO x-ray yield is also shown. This contribution was calculated using Meyerhof's prescription,[6] which has no fundamental significance, but can be used to describe the shape of the $1s\sigma$ MO x-ray yield (the magnitude is arbitrarily adjusted). The two-collision $1s\sigma$ MO x-ray yield is negligible in these collisions.

The agreement between the calculated intensity of MO x rays and experiment is fairly good in most cases. The experimental and calculated intensities are absolute, though in most cases the calculated yield is higher than the experimental yield. We have investigated the sensitivity of our calculations to the various approximations made. The most serious approximation is that Eq. (12) probably overestimates the $2p\sigma$ binding energy at intermediate distances. There is some evidence from relativistic Hartree-Fock calculations that $E_{2p\sigma}(R)$ is smaller at the extreme value.[23] This would give a smaller MO x-ray intensity in better agreement with experiment.

We have examined the questions posed in the Introduction. First, to see whether it is necessary to include the time dependence of $a(t)$, we performed separate calculations for 470-MeV Xe + Sn using

$$a(t) = \begin{cases} 0, & t<0 \\ a(\infty), & t>0. \end{cases} \quad (13)$$

No difference (within 20%) in the computed intensity of radiation between 35 and 60 keV was found. This justifies the approximation made by Heinig *et al.*[3] However, it is puzzling that this approximation is valid.

To describe one-collision $1s\sigma$ MO x rays, Thorson and Choi[5] write the probability amplitude as the sum of two parts: a "secular" part which is equivalent to the amplitude in Eq. (13), and a "transient" part which is a purely oscillatory function that approaches zero at $R=\infty$. For $1s\sigma$ MO

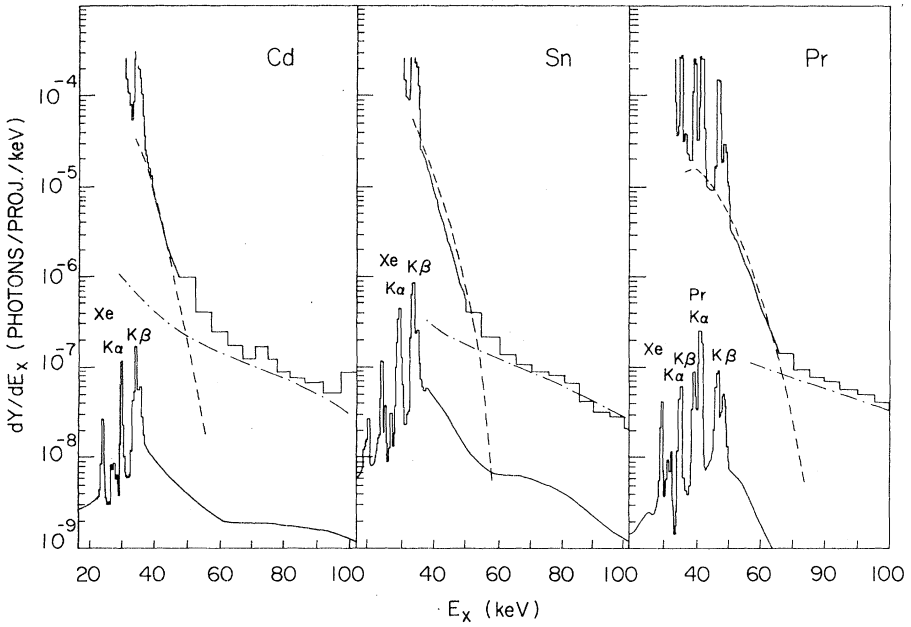

FIG. 5. Yields of continuum x rays observed in 470-MeV Xe + Cd, Sn, and Pr collisions. The calculated $2p\sigma$ (dashed) and $1s\sigma$ (dash-dot) MO x-ray yields are shown. Lower inset shows original spectrum (counts/channel, arbitrarily normalized), where a 0.75-g/cm^2 Cu absorber was used to attenuate low-energy radiation.

x rays, the transient part is orders of magnitude larger than the secular part during the collision and both contribute significantly to the MO x-ray yield. However, the transient $2p\sigma$ amplitude has only about the same magnitude as the secular $2p\sigma$ amplitude and apparently, does not contribute significantly to the MO x-ray yield, at least for x-ray energies beyond the UA L x-ray lines.

To study the projectile velocity dependence of $2p\sigma$ MO x-ray emission, we measured the Xe + Sn spectrum at 326 MeV also. The calculated and experimental radiation intensities per $2p\sigma$ vacancy are compared in Fig. 6 for 326- and 470-MeV Xe + Sn bombardments. The $1s\sigma$ MO x-ray yield has been subtracted in this figure. It is gratifying to see that although the calculated intensity is higher than the experimental one, the difference in the spectral shapes at the two different ion velocities is reproduced by the calculation. At lower velocities, the calculated and experimental intensities fall off faster. The difference between the shape of the experimental and theoretical yields at low x-ray energies is probably due to the Xe $K\beta$ line tailing into the continuum band.

The intensity difference between the spectra (per $2p\sigma$ vacancy) taken at the two energies is slight, despite the fact that the $2p\sigma$-vacancy cross section increases with the third to fifth power of the bombarding energy.[13] The relative insensitivity of the radiation intensity per $2p\sigma$ vacancy to bombarding energy, compared with the strong dependence of the $2p\sigma$ cross section on the bombarding energy,

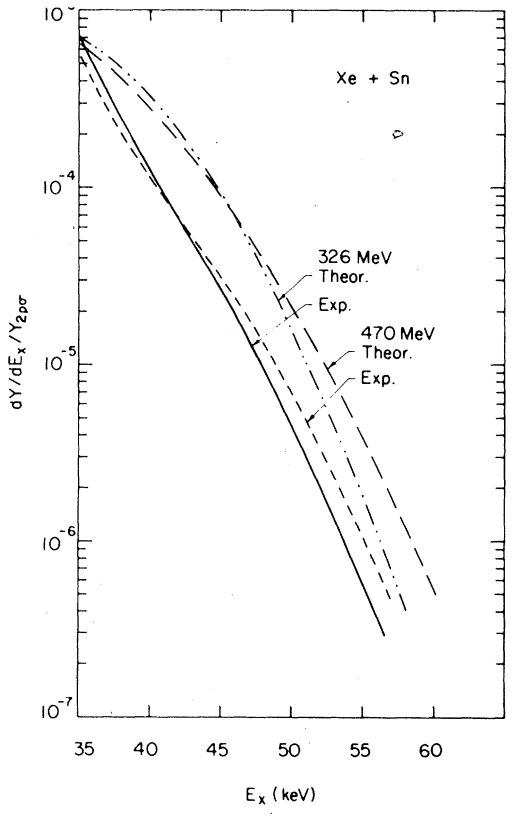

FIG. 6. Experimental thick-target yield of continuum x rays per $2p\sigma$ vacancy in 326- and 470-MeV Xe + Sn encounters is compared with the theoretically calculated radiation emitted per $2p\sigma$ vacancy.

justifies our approximate conversion of $(d\sigma/dE_x)/\sigma_{2p\sigma}$ to thick-target yields [Eq. (5)].

The impact-parameter dependence of the $2p\sigma$ MO x-ray yield is shown in Fig. 7. In this calculation, we integrated Eqs. (3) and (8) along Coulomb trajectories. The impact-parameter dependence of MO x-ray emission follows closely the impact-parameter dependence for the production of $2p\sigma$ vacancies. This suggests a further confirmation that the $C1$ x rays are due to $2p\sigma$ MO x-ray transitions could come from a study of the impact-parameter dependence $dP_x(b)/dE_x$. The kinematic peak at low impact parameters is a very distinctive feature of $2p\sigma$-$2p\pi$ rotational coupling and should be observed in $dP_x(b)/dE_x$ also. Such experimental studies have not been made thus far.

Our dynamical calculations predict broad peaks in the $2p\sigma$ continuum intensity near the higher-Z SA x-ray lines. These peaks are caused by the extremum in the $2p\sigma$ binding energy (in Xe+Sn, at $RZ_L = 3$ a.u., as one can see in Fig. 4). The quasistatic model[6,10] of MO x-ray emission predicts sharp peaks in the continuum yield where the derivative of the $2p\sigma$ binding energy approaches zero. In the dynamical calculations, the peaks are still present, but are much broader and less intense. In most of the encounters shown in Fig. 5, the x-ray lines emitted by the heavier collision partner obscure the peak in the MO x-ray yield. Fortuitously, this is usually the case. Those peaks may possibly be observed in highly asymmetric collisions where the x-ray lines emitted by the heavier collision partner are much weaker than in near symmetric collisions. For example, in 470-MeV Xe+Bi encounters the Bi K x rays come only from $1s\sigma$-vacancy formation, and are a factor of 10^{-2} less intense than the Xe K x-ray lines.

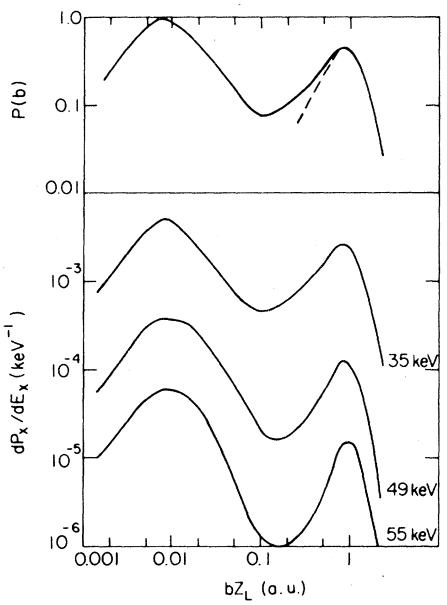

FIG. 7. Impact-parameter dependence of $2p\sigma$ MO x rays for 470-MeV Xe+Sn encounters. Top curve shows $P(b)$ for $2p\sigma$-$2p\pi$ rotational coupling. The kinematic peak is at $bZ_L \approx 0.01$ a.u. The dashed line was calculated using straight-line trajectories. The probability of x-ray emission per keV is given for E_x= 35, 49, and 55 keV.

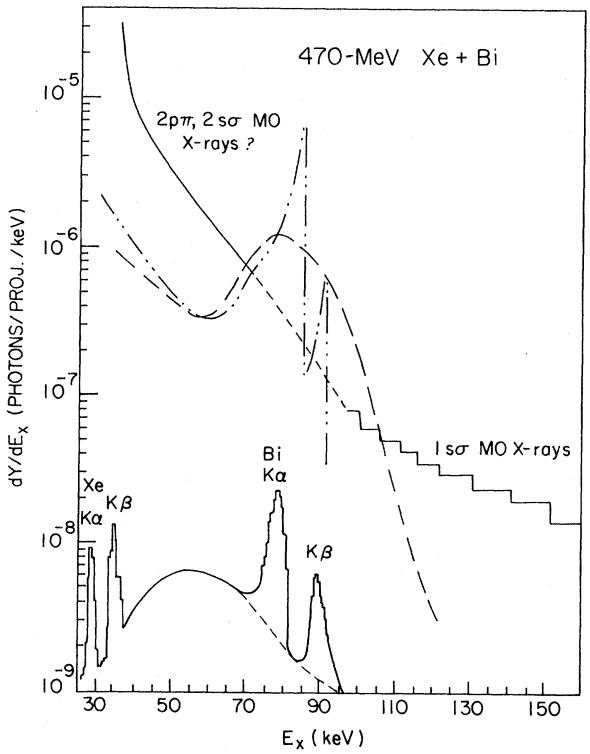

FIG. 8. Thick-target yield of continuum x rays in 470-MeV Xe+Bi collisions. The Bi K x-ray lines have been subtracted. Theoretical yields of $2p\sigma$ MO x rays calculated using Eq. (3) (long-dashed line) and the stationary phase approximation (dash-dot line) are shown (transitions from the two different energy levels, $3d\sigma/3d\pi$ and $4d\sigma/4d\pi$, each give one peak in the stationary phase approximation). Lower inset shows original spectrum (counts/channel, arbitrarily normalized) as in Fig. 5.

The experimental and calculated intensities of $2p\sigma$ MO x rays in 470-MeV Xe+Bi encounters are shown in Fig. 8. In the thick-target yield spectrum, the Bi K x-ray lines have been subtracted. The stationary phase or quasistatic model predictions are shown for comparison. The dynamical calculations are about a factor of 3 higher than the experimental yield. More importantly, no peak in the experimental yield is observed. The fact that

no peak is observed experimentally may not be serious. This spectrum has contributions from $2s\sigma$, $2p\pi$, and $1s\sigma$ MO x rays as well as $2p\sigma$ MO x rays (insert, Fig. 1). The $2s\sigma$ and $2p\pi$ MO x-ray spectra extend at least to 82 and 42 keV, respectively, but the x-ray intensities from these MO's have not been computed. The experimental spectrum may be explained by a weaker $2p\sigma$ MO x-ray yield than computed, plus contributions from $2s\sigma$ and $2p\pi$ MO x rays. In view of the uncertainty in the $2p\sigma$ binding energy curve in our calculations, a possible yield smaller by one-third is not unreasonable. We note that the calculated Xe + Sn yield is too high by a factor of 3 also (Fig. 6).

Still it is rather unusual that this peak has not been observed. We have searched for this peak in 470- and 625-MeV Xe + Ag, Sn, Pr, Sm, Ho, Ta, Au, Bi, and U encounters and in 200-MeV Kr + Zr and Pd encounters. It has not appeared anywhere. This may be because the peak is obscured by sharp K x-ray lines and by other continua in every case.

IV. CONCLUSIONS

The agreement between experiment and the computed intensity of $2p\sigma$ MO x rays in 470-MeV Xe collisions is sufficiently good to warrant the conclusion that the $C1$ continuum is due to $2p\sigma$ MO x rays. The dependence of the calculated MO x-ray yield on the time development of the amplitude for having created a $2p\sigma$ vacancy, on the ion velocity, and on the impact parameter has been examined.

The fact that a peak in the MO x-ray spectrum arising from the extremum in the $2p\sigma$ binding energy is predicted, but not observed remains a problem. More accurate calculations and a closer examination of the experimentally observed continuum intensity, which considers bremsstrahlung processes, as well as other K and L MO x rays, are needed.

---

*Supported in part by the National Science Foundation.

[1]P. Gippner, K.-H. Kaun, H. Sodan, F. Stary, W. Schulze, and Yu. P. Tretykov, Phys. Lett. 52B, 183 (1974).
[2]K. H. Heinig, H.-U. Jäger, H. Richter, and H. Woittennek, Phys. Lett. 60B, 249 (1976).
[3]K. H. Heinig, H.-U. Jäger, H. Richter, H. Woittennek, W. Frank, P. Gippner, K.-H. Kaun, and P. Manfrass J. Phys. B 10, 1321 (1977).
[4]W. Frank, P. Gippner, K.-H. Kaun, P. Manfrass, N. V. Pronin, and Yu. P. Tretykov, Z. Phys. A 279, 213 (1976).
[5]W. R. Thorson and J. H. Choi, Phys. Rev. A 15, 550 (1977).
[6]W. E. Meyerhof, T. K. Saylor, S. M. Lazarus, A. Little, B. B. Triplett, L. F. Chase, Jr., and R. Anholt, Phys. Rev. Lett. 32, 1279 (1974).
[7]K. M. Sando, Phys. Rev. A 9, 1103 (1974); J. C. Stewart, J. M. Peek, and J. Cooper, Astrophys. J. 179, 983 (1973).
[8]R. Anholt and W. E. Meyerhof (unpublished).
[9]V. Weisskopf, Phys. Z. 34, 1 (1933).
[10]J. H. Macek and J. S. Briggs, J. Phys. B 7, 1312 (1974).
[11]R. Anholt, J. Phys. B 9, L249 (1976).
[12]M. Gros and W. Greiner, Z. Phys. A 274, 165 (1975).
[13]W. E. Meyerhof, R. Anholt, T. K. Saylor, S. M. Lazarus, A. Little, and L. F. Chase, Jr., Phys. Rev. A 14, 1653 (1976).
[14]W. E. Meyerhof, R. Anholt, and T. K. Saylor, Phys. Rev. A 16, 169 (1977).
[15]W. N. Lennard and I. V. Mitchell, Nucl. Instrum. Methods 132, 39 (1976); J. Phys. B 9, L319 (1976); W. N. Lennard, I. V. Mitchell, J. S. Foster, and D. Phillips (unpublished).
[16]J. S. Briggs and K. Taulbjerg, J. Phys. B 8, 1909 (1975).
[17]J. S. Briggs and J. H. Macek, J. Phys. B 5, 579 (1972).
[18]K. Taulbjerg, J. S. Briggs, and J. Vaaben, J. Phys. B 9, 1351 (1976).
[19]R. Anholt, W. E. Meyerhof, and A. Salin, this issue, Phys. Rev. A 16, 951 (1977).
[20]S. S. Gershtein and V. D. Krivchenkov, Zh. Eksp. Teor. Fiz. 40, 149 (1961) [Sov. Phys. JETP 13, 1044 (1961)].
[21]K. Helfrich and H. Hartmann, Theor. Chim. Acta. 16, 263 (1970). We thank K. Helfrich for providing a copy of his computer code.
[22]J. H. Scofield, Phys. Rev. 179, 9 (1969).
[23]B. Fricke, T. Morovic, W.-D. Sepp, A. Rosén, and D. E. Ellis, Phys. Lett. 59A, 375 (1976); B. Fricke (private communication).